Available online at www.sciencedirect.com

ScienceDirect

IFAC PapersOnLine CONFERENCE PAPER ARCHIVE

IFAC PapersOnLine 58-30 (2024) 73–78

# Switched Kinematic and Indirect Force Control of a Motorized Ankle Orthosis To Perturb the Ankle Joint During Walking*

**Nicholas Rubino**[1], **Miguel Manchola**[1], **Victor H. Duenas**[1]

[1] *Department of Mechanical and Aerospace Engineering, Syracuse University, 13244 NY, USA.(e-mail:{narubino, mdmancho, vhduenas}@syr.edu).*

**Abstract:** People post-stroke walk with unnatural gait patterns due to reduced propulsion and muscle weakness in their affected leg. Powered exoskeletons can provide gait assistance to improve their walking speed and endurance. However, these robotic devices usually provide assistive torques to emulate healthy gait patterns and biological joint moments that do not directly translate to improving muscle capacity and propulsion. Alternatively, applying safe kinematic perturbations about joints at discrete instances in the step cycle can aid to target muscles, such as the ankle plantarflexors or the soleus muscle, and thus, improve propulsion during walking. This paper develops two closed-loop controllers for a motorized ankle-foot orthosis with a cable-driven mechanism that strategically perturbs the ankle joint during the loading phase of walking, which is the region where the soleus muscle is naturally most active. First, a *nonlinear tensioning controller* is developed to build tension in the cable mechanism and prevent slackness in the early stance phase. The tensioning controller is activated at heel strike and tracks a desired electric motor trajectory generated by an admittance model. Then, a *joint perturbation controller* is developed to apply kinematic deviations (perturbations) to the ankle joint in the mid-late stance (loading) phase of walking to evoke changes in the soleus muscle activity. A Lyapunov-based stability analysis is developed independently for each controller ensuring exponential tracking in their respective regions of the step cycle.



*Keywords:* Nonlinear control, Exoskeletons, Assistive devices

## 1. INTRODUCTION

Stroke survivors experience diminished muscle capacity and propulsion that limit their endurance and walking ability Weerdesteyn et al. (2008). In particular, the plantarflexors including the soleus muscle are critical for walking as they produce the majority of propulsive force during the mid-late stance phase (i.e., at "push-off") Winter (2009). Lower-limb exoskeletons can help people with stroke during neurorehabilitation for improving gait speed, endurance, and the energetic costs of walking Awad et al. (2020). However, traditional robotic exoskeletons usually assist stroke survivors by replicating natural gait patterns or biological joint torques Gandolla et al. (2018). Further, human-in-the-loop exoskeleton controllers have been developed to improve the gait energetics of people post-stroke Walsh (2018). However, such approaches that emulate healthy gait patterns or optimize the gait energetics do not directly improve muscle function and propulsion. Therefore, alternative control strategies are needed for robotic exoskeletons to target joints and muscles in new ways that enhance propulsion and muscle activation levels during walking.

Mechanical manipulation of the ankle joint through applying controlled rotational perturbations is a potential strategy to target the plantarflexors during push-off. Imposing perturbations or deviations from the user's natural joint kinematics can be used to generate shifts from the baseline muscle activity while walking. The human neurophysiology community has developed open-loop approaches to elicit increments to the soleus muscle responses (with respect to the baseline) measured using surface electromyography (EMG) Mazzaro et al. (2005). However, closed-loop control methods are motivated to develop customized neurorehabilitation programs that account for differences in muscle capacity and gait patterns across participants. Such closed-loop controllers can be implemented in robotic exoskeletons and motorized orthoses to target and potentially modulate the soleus muscle activity, while ensuring safety of the participant. Recently, an integral-like EMG error system was used to design an adaptive backstepping controller by prescribing a desired muscle activation level Rubino et al. (2023). Different from this EMG-based approach that can be prone to sensor noise during walking, the motivation in this paper is to impose kinematic

*Research reported in this publication was supported in part by the National Science Foundation under Grant No. 2218913 and by pilot funding from the National Institutes of Health National Center of Neuromodulation for Rehabilitation, the National Center for Complementary and Integrative Health, the National Institute on Deafness and Other Communication Disorders, and the National Institute of Neurological Disorders and Stroke; NIH/NICHD Grant Number P2CHD086844 which was awarded to the Medical University of South Carolina. The contents are solely the responsibility of the authors and do not necessarily represent the official views of the NSF, NIH or NICHD.


10.1016/j.ifacol.2025.01.159

perturbations using the ankle joint angular position and velocity to evoke changes in the soleus muscle responses.

In this paper, the main contribution is the design of two closed-loop controllers that actuate a powered cable-driven ankle-foot orthosis. The controllers are implemented in separate regions of the stance phase of walking to apply tension to the Bowden cable mechanism using an electric motor, which is offloaded away from the body, and target the soleus muscle to increment its activation. First, in early stance phase, a robust indirect force controller referred to as the *tensioning controller* is designed to mitigate cable slackness, which is detrimental to achieve suitable tracking performance. The tensioning controller tracks desired electric motor trajectories generated by an admittance model that leverages cable tension feedback. Then, in the mid-late stance phase, a *perturbation controller* is designed to perturb the ankle joint. The perturbations are prescribed deviations from the natural ankle joint kinematics to modulate the soleus muscle activity output, which can be used as a gait rehabilitation tool. An Euler-Lagrange dynamic system is used to model the uncertain nonlinear single degree-of-freedom motorized ankle-foot orthosis and muscle-tendon. Piecewise constant switching signals are generated using heel and toe ground reaction forces to turn on the tensioning controller during early stance and the perturbation controller during mid-late stance, respectively. Exponential tracking is obtained for each controller independently within their activation regions.

## 2. DYNAMICS

### 2.1 Ankle-Foot Orthosis Dynamics

The single degree-of-freedom ankle joint muscle-tendon and powered foot orthosis system is modeled with the following dynamics

$$J\ddot{q}(t) + f(q,\dot{q}) + G(q) + d(t) = \tau(t), \tag{1}$$

where $q : \mathbb{R}_{\geq t_0} \to \mathcal{Q}$ denotes the measurable ankle joint angular position, $\mathcal{Q} \subset \mathbb{R}$ denotes the set of ankle joint angles, and $t_0 \in \mathbb{R}$ is the initial time; $\dot{q}, \ddot{q} : \mathbb{R}_{\geq t_0} \to \mathbb{R}$ denote the measurable ankle angular velocity and unmeasurable angular acceleration, respectively; $J \in \mathbb{R}_{>0}$ denotes the uncertain positive inertia constant of the overall ankle-foot orthosis system; the nonlinear function $f : \mathcal{Q} \times \mathbb{R} \to \mathbb{R}$ denotes the elasticity due to the joint stiffness and the viscous effects due to damping in the musculotendon complex and is defined as $f \triangleq K_1 \exp(-K_2 q)(q - K_3) - B_1 \tanh(-B_2\dot{q}) + B_3\dot{q}$, where $K_1, K_2, K_3, B_1, B_2, B_3 \in \mathbb{R}_{>0}$ are uncertain positive constants described in Downey et al. (2017); Riener et al. (2000); Schauer et al. (2005); $G : \mathcal{Q} \to \mathbb{R}$ denotes the effects of gravity and is defined as $G \triangleq mgl\sin(q)$, where $m \in \mathbb{R}_{>0}$ is the combined mass of the foot and orthosis, $g \in \mathbb{R}$ is the acceleration due to gravity, and $l \in \mathbb{R}_{>0}$ is the distance between the ankle joint and the lumped center of the mass of the ankle-foot orthosis; and $d : \mathbb{R}_{\geq t_0} \to \mathbb{R}$ denotes an external exogenous disturbance including unmodeled effects in the musculoskeletal system. The torque applied by the electric motor about the ankle joint is denoted by $\tau : \mathbb{R}_{\geq t_0} \to \mathbb{R}$ and is defined as

$$\tau(t) \triangleq \sigma_p B_e u_e(t), \tag{2}$$

where $u_e : \mathbb{R}_{\geq t_0} \to \mathbb{R}$ is the motor current control input, $B_e \in \mathbb{R}_{>0}$ is the unknown positive constant control effectiveness, and $\sigma_p \in \{0,1\}$ is a piecewise constant switching signal developed to apply an ankle joint perturbation per step cycle within the mid-late stance phase of walking and thus, target the soleus muscle.

### 2.2 Electric Motor Dynamics

To develop the cable tensioning controller to mitigate cable slackness, the electric motor system is modeled with the following dynamics Chang et al. (2023)

$$J_m\ddot{\theta}_m(t) + b_m\dot{\theta}_m(t) + d_m(t) = B_e\sigma_m u_m(t), \tag{3}$$

where $\theta_m, \dot{\theta}_m, \ddot{\theta}_m : \mathbb{R}_{\geq t_0} \to \mathbb{R}$ denote the measurable angular position and velocity, and unmeasurable angular acceleration of the electric motor, respectively; $J_m, b_m \in \mathbb{R}_{\geq 0}$ are the unknown positive constant inertia and damping coefficient; $d_m : \mathbb{R}_{\geq t_0} \to \mathbb{R}$ denotes unmodeled disturbances; $u_m : \mathbb{R}_{\geq t_0} \to \mathbb{R}$ is the subsequently designed motor control input to mitigate cable slackness; and $\sigma_m \in \{0,1\}$ is a piecewise constant switching signal designed to turn the tensioning controller on during the early stance.

The following assumptions and properties are exploited in the subsequent control design and stability analysis.

*Assumption 1.* The additive disturbances $d$ and $d_m$ are bounded as $|d| \leq \zeta_d$ and $|d_m| \leq \zeta_{d_m}$, where $\zeta_d, \zeta_{d_m} \in \mathbb{R}_{>0}$ are known positive constants.

*Assumption 2.* The desired ankle trajectory $q_d \in \mathbb{R}$ (i.e., the ankle perturbations) and its time derivatives $\dot{q}_d, \ddot{q}_d \in \mathbb{R}$ are designed to be bounded by known positive constants such as $|q_d| \leq \zeta_1, |\dot{q}_d| \leq \zeta_2, |\ddot{q}_d| \leq \zeta_3$ and $\zeta_1, \zeta_2, \zeta_3 \in \mathbb{R}_{>0}$.

*Property 1.* $|G(q)| \leq \overline{g}$, where $\overline{g} \in \mathbb{R}_{>0}$ is a known constant (Lewis et al., 2003, Ch. 3).

*Property 2.* The control effectiveness is bounded as $c_e \leq B_e \leq c_E$, where $c_e, c_E \in \mathbb{R}_{>0}$ are known constants.

The ankle joint angular position and velocity $q, \dot{q}$ and electric motor angular position and velocity $\theta_m, \dot{\theta}_m$ are depicted in Fig. 1 along with the ankle-foot orthosis system.

### 2.3 Switching Signals

In this section, piecewise constant switching signals $\sigma_p, \sigma_m \in \{0,1\}$ are defined to activate the ankle perturbation controller $u_e$ and cable tensioning controller $u_m$ in the mid-late stance and early stance phase of walking, respectively. The switching signals are defined using a gait-phase detection algorithm that exploits heel and toe ground reaction force measurements from sensors embedded in the sole of the orthosis $x_1, x_2 : \mathbb{R}_{\geq t_0} \to \mathbb{R}_{>0}$. The switching signals $\sigma_p, \sigma_m$ are defined as

$$\sigma_p(t) \triangleq \begin{cases} 1, & t \in \mathcal{P} \\ 0, & t \notin \mathcal{P} \end{cases}, \quad \sigma_m(t) \triangleq \begin{cases} 1, & t \in \mathcal{M} \\ 0, & t \notin \mathcal{M} \end{cases}, \tag{4}$$

where $\mathcal{P}$ denotes the ankle perturbation set (i.e., the perturbation region within the step cycle) and $\mathcal{M}$ denotes the cable tensioning set (i.e., the region within the step

cycle in which the cable tensioning controller is applied). The sets $\mathcal{P}, \mathcal{M}$ are defined as

$$\mathcal{P} \triangleq \{t \in \mathbb{R}_{\geq t_0} \mid (x_1(t) \geq \underline{x}) \wedge (x_2(t) > \overline{x})\}, \quad (5)$$

$$\mathcal{M} \triangleq \{t \in \mathbb{R}_{\geq t_0} \mid (x_1(t) \geq \underline{x}) \wedge (x_2(t) \leq \overline{x})\}, \quad (6)$$

where $\underline{x}, \overline{x} \in \mathbb{R}_{>0}$ denote the selected lower and upper thresholds of ground reaction forces, respectively. The thresholds defining $\mathcal{M}$ describe the early stance, where the heel force is greater or equal to the lower threshold and the toe force is less than or equal to the upper threshold. The set $\mathcal{P}$ denotes the mid-late stance, where the soleus muscle is most active and can be targeted using the perturbation controller when the toe force is greater than the upper threshold. Defining these switching signals ensures the controllers are never active simultaneously, preventing counteracting inputs.

## 3. CONTROL DEVELOPMENT

In this section, the two closed-loop controllers: the ankle joint perturbation controller and the cable tensioning controller are designed leveraging the ankle-foot orthosis dynamics in (1) and the electric motor dynamics in (3).

### *3.1 Ankle Joint Perturbation Controller Design*

The control objective is to track desired ankle joint angular trajectories (i.e., to apply joint perturbations) within the mid-late stance phase of walking during the perturbation region ($\sigma_p = 1$). To facilitate the following control design, a measurable angular joint position error $e : \mathbb{R}_{\geq t_0} \to \mathbb{R}$ and an auxiliary filtered tracking error $r : \mathbb{R}_{\geq t_0} \to \mathbb{R}$ are defined as

$$e(t) = q_d(t) - q(t), \quad (7)$$

$$r(t) = \dot{e}(t) + \alpha e(t), \quad (8)$$

where $\alpha \in \mathbb{R}_{>0}$ is a selectable constant control gain and $q_d : \mathbb{R}_{\geq t_0} \to \mathbb{R}$ is the desired ankle kinematic trajectory (i.e., the perturbation profile). The open-loop kinematic error system is obtained by pre-multiplying the time derivative of (8) by $J$, substituting for (1), (7) and (8), and performing further algebraic manipulation yields

$$J\dot{r} = J\ddot{q}_d + f(q, \dot{q}) + G(q) + d - \tau + J\alpha r - J\alpha^2 e. \quad (9)$$

The closed-loop dynamics can be segregated into terms that can be upper bounded by a constant and terms that can be upper bounded by a state-dependent function. The following auxiliary signals $W_d : \mathbb{R}_{\geq t_0} \to \mathbb{R}$, $N_d : \mathbb{R}_{\geq t_0} \to \mathbb{R}$, and $\tilde{N} : \mathbb{R}_{\geq t_0} \to \mathbb{R}$ are defined as

$$W_d \triangleq f(q_d, \dot{q}_d) + G(q_d), \quad (10)$$

$$N_d \triangleq d + J\ddot{q}_d + f(q_d, \dot{q}_d) + G(q_d), \quad (11)$$

$$\tilde{N} \triangleq f(q, \dot{q}) - f(q_d, \dot{q}_d) + G(q) - G(q_d) + J\alpha r - J\alpha^2 e + e. \quad (12)$$

Using Assumption 1 and exploiting that $|W_d| \leq \beta_d$, $\beta_d \in \mathbb{R}_{>0}$, the auxiliary signal in (11) can be upper bounded as

$$|N_d| \leq \xi_d, \quad (13)$$

where $\xi_d \in \mathbb{R}_{>0}$ is a known positive constant. By using Property 1, (7), (8), and the Mean Value Theorem, an upper bound for (12) can be developed as

$$|\tilde{N}| \leq \varrho(||z||)||z||, \quad (14)$$

where $z : \mathbb{R}_{\geq t_0} \to \mathbb{R}^2$ is defined as $z \triangleq [\, e \; r \,]^T$, and $\varrho : \mathbb{R} \to \mathbb{R}$ is a known positive, non-decreasing, radially unbounded function. Given the open-loop error system in (9), the ankle pertubation control input is designed as

$$u_e \triangleq k_1 r + k_2 \text{sgn}(r) + k_3 \varrho^2(\|z\|) r, \quad (15)$$

where $k_1, k_2, k_3 \in \mathbb{R}_{>0}$ are selectable positive gain constants, and $\text{sgn}(\cdot) : \mathbb{R} \to [-1, 1]$ is the signum function. The electric motor control input in (15) includes a position-velocity feedback term, a sliding-mode term to compensate for the constant upper bound in (13), and a nonlinear damping term to compensate for the state-dependent upper bound in (14). The closed-loop kinematic error system is obtained by substituting (15) and (2) with $\sigma_p = 1$ into (9) and using the definitions in (11) and (12) as

$$J\dot{r} = \tilde{N} + N_d - e - B_e\Big(k_1 r + k_2 \text{sgn}(r) + k_3 \varrho^2(\|z\|) r\Big). \quad (16)$$

### *3.2 Cable Tensioning Controller Design*

The cable tensioning objective is designed to mitigate slackness during the early stance before applying the perturbation control input. To quantify the performance of the tensioning objective, the measurable position error $\eta : \mathbb{R}_{\geq t_0} \to \mathbb{R}$ and filtered tracking error $\nu : \mathbb{R}_{\geq t_0} \to \mathbb{R}$ are defined as

$$\eta(t) = \theta_d(t) - \theta_m(t), \quad (17)$$

$$\nu(t) = \dot{\eta}(t) + \alpha_m \eta(t), \quad (18)$$

where $\theta_d, \dot{\theta}_d, \ddot{\theta}_d \in \mathbb{R}$ are the desired, bounded motor angular position, velocity and acceleration, respectively, and $\alpha_m \in \mathbb{R}_{>0}$ is a positive constant selectable gain. The desired position, velocity, and acceleration of the motor are generated using the following admittance model

$$J_d\ddot{\theta}_d + B_d\dot{\theta}_d + K_d\theta_d = \text{sat}_{\beta_1}(T_m - T_d), \quad (19)$$

where $J_d, B_d, K_d \in \mathbb{R}_{>0}$ are the desired virtual mass, damper, and stiffness parameters that are selected such that the transfer function of (19) is passive H. K. Khalil (2002); $T_d \in \mathbb{R}$ is the desired bounded, smooth cable tension; $T_m \in \mathbb{R}$ is the measurable cable tension; and $\beta_1 \in \mathbb{R}$ is a saturation limit. Taking the time derivative of (18), premultiplying by $J_m$, substituting for (3) and (18), and performing some algebraic manipulation yields

$$J_m\dot{\nu} = J_m\ddot{\theta}_d + b_m\dot{\theta}_m + d_m - B_e\sigma_m u_m + J_m\alpha_m\nu - J_m\alpha_m^2\eta. \quad (20)$$

To facilitate the subsequent control design and stability analysis, the auxillary signal $\chi_m : \mathbb{R}_{\geq t_0} \to \mathbb{R}$ is defined as

$$\chi_m = J_m(\ddot{\theta}_d + \alpha_m\nu - \alpha_m^2\eta) + b_m\dot{\theta}_m + d_m + \eta. \quad (21)$$

Exploiting Assumption 1, (17), (18), and passivity of the admittance model in (19), an upper bound for $\chi_m$ can be obtained as

$$|\chi_m| \leq \rho_1 + \rho_2||\psi_m||, \quad (22)$$

where $\rho_1, \rho_2 \in \mathbb{R}_{>0}$ are known constants and $\psi_m : \mathbb{R}_{\geq t_0} \to \mathbb{R}^2$ is a composite vector of the error signals defined as $\psi_m \triangleq [\, \eta \; \nu \,]^T$. Given the open-loop error system in (20), the cable tensioning control input is designed as

$$u_m = k_4\nu + (k_5 + k_6||\psi_m||)\text{sgn}(\nu), \quad (23)$$

where $k_4, k_5, k_6 \in \mathbb{R}_{>0}$ are positive selectable control gains. The closed-loop error system is obtained by substituting (21) and (23) into (20) and setting $\sigma_m = 1$

$$J_m\dot{\nu} = \chi_m - B_e\Big(k_4\nu + (k_5 + k_6||\psi_m||)\text{sgn}(\nu)\Big) - \eta. \quad (24)$$

## 4. STABILITY ANALYSIS

The stability of the closed-loop ankle perturbation controller to impose joint perturbations during the mid-late stance phase can be examined using Theorem 1. Moreover, the stability of the closed-loop tensioning controller implemented in early stance can be examined using Theorem 2.

*Theorem 1.* Given the closed-loop error system in (16), the controller in (15) ensures global exponential kinematic tracking within the perturbation region (i.e. mid-late stance phase of walking) in the sense that

$$\|z(t)\| \leq \sqrt{\frac{\lambda_2}{\lambda_1}}\|z(t_0)\|e^{-\frac{\delta}{4\lambda_2}(t-t_0)}, \tag{25}$$

provided the following sufficient gain conditions are satisfied

$$k_2 \geq \frac{\xi_d}{c_e}, \delta \triangleq \min\{\alpha, k_1 c_e\} > \frac{1}{2k_3 c_e}. \tag{26}$$

**Proof.** Let $V : \mathbb{R}^2 \times \mathbb{R}_{\geq t_0} \to \mathbb{R}$ be a positive definite, radially unbounded, continuously differentiable Lyapunov function candidate defined as

$$V \triangleq \frac{1}{2}e^2 + \frac{1}{2}Jr^2. \tag{27}$$

The function in (27) satisfies the following inequalities

$$\lambda_1\|z\|^2 \leq V(z,t) \leq \lambda_2\|z\|^2, \tag{28}$$

where $\lambda_1 \triangleq \min(\frac{1}{2}, \frac{\underline{J}}{2})$ and $\lambda_2 \triangleq \max(\frac{1}{2}, \frac{\overline{J}}{2})$, where $\underline{J}, \overline{J} \in \mathbb{R}_{>0}$ are positive constant bounds of the system's inertia $J$. Let $z(t)$ be a Filippov solution to the differential inclusion $\dot{z} \in K[h](z)$, where $K[h](\cdot)$ is defined as in Filippov (1964), and $h$ is defined by using (8) and (16) as $h \triangleq [\, h_1 \;\; h_2 \,]$, where

$h_1 \triangleq r - \alpha e$,

$h_2 \triangleq \frac{1}{J}\{\tilde{N} + N_d - e - B_e\big(k_1 r + k_2 \text{sgn}(r) + k_3 \varrho^2(\|z\|)r\big)\}$.

The control input in (15) has the signum function; hence, the time derivative of (27) exists almost everywhere (a.e.), i.e., for almost all $t$. Based on (Fischer et al., 2013, Lemma 2), $\dot{V}(z,t) \overset{a.e.}{\in} \dot{\tilde{V}}(z,t)$, where $\dot{\tilde{V}}$ is the generalized time derivative of (27) along the Filippov trajectories of $\dot{z} = h(z)$ and is defined in Fischer et al. (2013) as $\dot{\tilde{V}} \triangleq \bigcap_{\xi \in \partial V} \xi^T K\,[\, \dot{e} \;\; \dot{r} \;\; 1 \,]^T\,(e,\, r,\, t)$, where $\partial V(z,t)$ is the generalized gradient of $V$ at $(z,t)$. Since $V(z,t)$ is continuously differentiable in $z$, $\partial V = \{\nabla V\}$, $\dot{\tilde{V}} \overset{a.e.}{\subset} [\, e \;\; Jr \,] K\,[\, \dot{e} \;\; \dot{r} \,]^T$. Therefore, after substituting (8) and (16), canceling common terms, the generalized time derivative of (27) can be expressed as

$$\dot{\tilde{V}} \overset{a.e.}{\subset} -\alpha e^2 + r\big(\tilde{N} + N_d - B_e(k_1 r + k_2 K[\text{sgn}(r)] + k_3 \varrho^2(\|z\|)r)\big), \tag{29}$$

where $K[\text{sgn}(r)] = \text{SGN}(r)$ such that $\text{SGN}(r) = 1$ if $r > 0$, $[-1, 1]$ if $r = 0$, and $-1$ if $r < 0$. Substituting the upper bounds obtained in (13) and (14), and using Property 2, the previous expression can be upper bounded as

$$\dot{\tilde{V}} \overset{a.e.}{\leq} -\alpha e^2 - k_1 c_e r^2 - (k_2 c_e - \xi_d)|r| + \varrho(\|z\|)\|z\||r| - k_3 c_e \varrho^2(\|z\|)r^2. \tag{30}$$

By completing the squares for the last two terms in the previous inequality, (30) can be rewritten as

$$\dot{\tilde{V}} \overset{a.e.}{\leq} -\alpha e^2 - k_1 c_e r^2 - (k_2 c_e - \xi_d)|r| + \frac{1}{4k_3 c_e}\|z\|^2. \tag{31}$$

Provided the gain conditions in (26) are satisfied, the inequality in (31) can be further upper bounded as

$$\dot{\tilde{V}} \overset{a.e.}{\leq} -\frac{\delta}{2}\|z\|^2 - \Big(\frac{\delta}{2} - \frac{1}{4k_3 c_e}\Big)\|z\|^2. \tag{32}$$

Using the inequalities in (28) and (32) and solving the differential inequality yields (25). Since $V > 0$ and $\dot{V} \overset{a.e.}{\leq} 0$, $V \in \mathcal{L}_\infty$; hence, $e, r \in \mathcal{L}_\infty$, which implies that $z \in \mathcal{L}_\infty$, and thus $u_e \in \mathcal{L}_\infty$ in (15) and $\tau \in \mathcal{L}_\infty$ in (2). Since $e, r \in \mathcal{L}_\infty$, then $\dot{e} \in \mathcal{L}_\infty$ from (8), and hence $q, \dot{q} \in \mathcal{L}_\infty$, which implies $\ddot{q} \in \mathcal{L}_\infty$ from (1).

*Theorem 2.* Given the closed-loop error system in (24), the robust tensioning controller in (23) achieves global exponential tracking in the sense that

$$|\eta(t)| \leq \sqrt{\frac{\lambda_4}{\lambda_3}}|\eta(0)|e^{-\frac{\delta_m}{2\lambda_4}(t-t_0)}, \tag{33}$$

provided the following sufficient gain conditions are satisfied

$$k_5 \geq \frac{\rho_1}{c_e}, k_6 \geq \frac{\rho_2}{c_e}. \tag{34}$$

**Proof.** Let $V_2 : \mathbb{R}_{\geq t_0} \to \mathbb{R}$ be a positive-definite continuously differentiable Lyapunov function candidate defined as

$$V_2 \triangleq \frac{1}{2}\eta^2 + \frac{1}{2}J_m\nu^2, \tag{35}$$

that satisfies the following inequalities

$$\lambda_3||\psi_m||^2 \leq V_2(\psi_m, t) \leq \lambda_4||\psi_m||^2, \tag{36}$$

where $\lambda_3 = \min\{\frac{1}{2}, \frac{\underline{J}_m}{2}\}$, and $\lambda_4 = \max\{\frac{1}{2}, \frac{\overline{J}_m}{2}\}$, where $\underline{J}_m, \overline{J}_m \in \mathbb{R}_{>0}$ are constant bounds. Using a similar procedure as for Theorem 1, the generalized time derivative of (35) can be obtained after substituting (18) and (24) as

$$\dot{\tilde{V}}_2 \overset{a.e.}{\subset} -\alpha_m\eta^2 + \nu\chi_m - B_e k_4\nu^2 - B_e(k_5 + k_6||\psi_m||)\nu K[\text{sgn}(\nu)]. \tag{37}$$

Substituting for (22), an upper bound for the previous expression can be obtained as

$$\dot{\tilde{V}}_2 \overset{a.e.}{\leq} -\alpha_m\eta^2 - k_4 c_e\nu^2 - (k_5 c_e - \rho_1)|\nu| - (k_6 c_e - \rho_2)|\nu|||\psi_m||. \tag{38}$$

Provided the sufficient gain conditions in (34) are satisfied, the previous inequality can be further upper bounded as

$$\dot{\tilde{V}}_2 \overset{a.e.}{\leq} -\alpha_m\eta^2 - k_4 c_e\nu^2 \overset{a.e.}{\leq} -\delta_m||\psi_m||^2, \tag{39}$$

where $\delta_m \triangleq \min\{\alpha_m, k_4 c_e\}$. Using (36) and (39), the exponential result in (33) can be obtained. Since $V_2 > 0$ and $\dot{V}_2 \overset{a.e.}{\leq} 0$, $V_2 \in \mathcal{L}_\infty$. Thus, $\eta, \nu \in \mathcal{L}_\infty$ and from (23), $u_m \in \mathcal{L}_\infty$. Since $\eta, \nu \in \mathcal{L}_\infty$, then $\dot{\eta} \in \mathcal{L}_\infty$ in (18), and hence $\theta_m, \dot{\theta}_m \in \mathcal{L}_\infty$, which implies that $\ddot{\theta}_m \in \mathcal{L}_\infty$ in (3).

## 5. APPARATUS

The apparatus, depicted in Fig. 1, consists of a customized powered ankle-foot orthosis designed to fit various foot sizes and is affixed to the participant using straps around the shank and foot. The device is driven by a cable actuation system as in Andersen and Sinkjær (2003). A 24 VDC brushless electric motor (Maxon) is mounted on a separate actuation unit to apply torque about the

ankle joint using a Bowden cable mechanism. The cable tension is measured using an inline load cell (Omega) placed in the Bowden cable connecting the orthosis and the electric motor. The ankle joint angular position and velocity are measured and computed, respectively using an optical encoder (US Digital) mounted on the orthosis. Toe and heel ground reaction forces are read using force sensitive resistors (FlexiForceA401) embedded in the sole of the orthosis. Soleus surface EMG measurements were collected using two 0.875 x 1.375 inch electrode pads (13-NEURO PLUS A10041-60) placed two inches apart along the centerline of the shank below the head of the gastrocnemius, and are connected to an amplifier (Bortec AMT-8). The controllers are implemented using a desktop computer (Windows 10 OS) running a real-time target (QUARC 2.6, Quanser) using MATLAB/Simulink 2018a (Mathworks). A treadmill (NordicTrack T7.5S) is used for walking and a closed-loop controller is implemented to achieve the desired self-selected constant walking speed. To ensure participant safety, an emergency stop button is available and software stop conditions limit the angular position of the ankle device and current supplied to the motor.

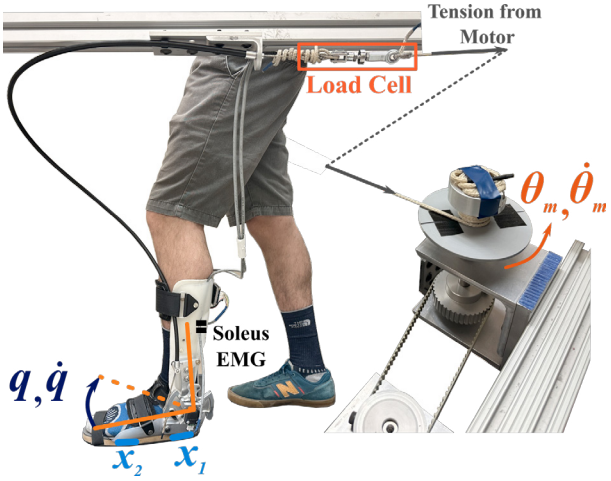


Fig. 1. The powered cable-driven ankle-foot orthosis. The load cell is in line with the actuation cable between the device and electric motor, which applies torque about the ankle joint. The load cell is used for cable tensioning feedback. The electric motor pulls the cable, rotating the ankle joint in the direction of $q, \dot{q}$ (measured by an optical encoder aligned with the ankle in the sagittal plane) to perturb the joint in mid-late stance. The angular position and velocity, $\theta_m, \dot{\theta}_m$, of the electric motor are measured using an optical encoder mounted along the electric motor's drive shaft to implement the tensioning controller in early stance phase. EMG pads are placed on the surface of the skin to collect soleus muscle activity. Heel and toe ground reaction forces, depicted by $x_1, x_2$, respectively, are measured using force sensitive resistors embedded in the sole of the device.

## 6. CONCLUSION

In this paper, two closed-loop nonlinear robust controllers were designed and analyzed to control a motorized ankle-foot orthosis with a cable-driven mechanism to target the ankle joint and the soleus muscle during treadmill walking. First, a cable tensioning controller was developed for mitigating cable slackness in the early stance phase. The cable tensioning controller exploited an admittance model for indirect force control. Then, an ankle perturbation controller was designed to target the soleus muscle in the mid-late stance phase by tracking a kinematic trajectory. A Lyapunov-based stability analysis was developed for each controller to ensure exponential tracking. Future work includes the implementation of the controllers with people post-stroke, who may experience benefits in propulsion due to increasing soleus muscle activation.

## REFERENCES

Andersen, J.B. and Sinkjær, T. (2003). Mobile ankle and knee perturbator. *IEEE Transactions on Biomedical Engineering*, 50(10), 1208–1211. doi: 10.1109/TBME.2003.816073.

Awad, L.N., Kudzia, P., Revi, D.A., Ellis, T.D., and Walsh, C.J. (2020). Walking faster and farther with a soft robotic exosuit: Implications for post-stroke gait assistance and rehabilitation. *IEEE Open Journal of Engineering in Medicine and Biology*, 1, 108–115. doi: 10.1109/OJEMB.2020.2984429.

Chang, C., Casas, J., and Duenas, V.H. (2023). Closed-loop kinematic and indirect force control of a cable-driven knee exoskeleton: A lyapunov-based switched systems approach. *IEEE Open Journal of Control Systems*, 2, 171–184. doi:10.1109/OJCSYS.2023.3289771.

Downey, R.J., Cheng, T.H., Bellman, M.J., and Dixon, W.E. (2017). Switched tracking control of the lower limb during asynchronous neuromuscular electrical stimulation: Theory and experiments. *IEEE Transactions on Cybernetics*, 47(5), 1251–1262. doi: 10.1109/TCYB.2016.2543699.

Filippov, A.F. (1964). Differential equations with discontinuous right-hand side. In *Fifteen papers on differential equations*, volume 42 of *American Mathematical Society Translations - Series 2*, 199–231. American Mathematical Society.

Fischer, N., Kamalapurkar, R., and Dixon, W.E. (2013). LaSalle-Yoshizawa corollaries for nonsmooth systems. *IEEE Transactions on Automatic Control*, 58(9), 2333–2338. doi:10.1109/TAC.2013.2246900.

Gandolla, M., Guanziroli, E., D'Angelo, A., Cannaviello, G., Molteni, F., and Pedrocchi, A. (2018). Automatic setting procedure for exoskeleton-assisted overground gait: Proof of concept on stroke population. *Frontiers in Neurorobotics*, 12(MAR). doi:10.3389/fnbot.2018.00010.

H. K. Khalil (2002). *Nonlinear Systems*. Prentice Hall, 3 edition.

Lewis, F.L., Dawson, D.M., and Abdallah, C.T. (2003). *Robot Manipulator Control*.

Mazzaro, N., Grey, M.J., and Sinkjær, T. (2005). Contribution of afferent feedback to the soleus muscle activity during human locomotion. *Journal of Neurophysiology*, 93(1), 167–177. doi:10.1152/jn.00283.2004.

Riener, R., Ferrarin, M., Pavan, E.E., and Frigo, C.A. (2000). Patient-driven control of FES-supported standing up and sitting down: Experimental results. *IEEE Transactions on Rehabilitation Engineering*, 8(4), 523–529. doi:10.1109/86.895956.

Rubino, N., Lawler, E., Casas, J., and Duenas, V.H. (2023). Backstepping control of a motorized ankle orthosis targeting the soleus muscle during walking. In *IFAC-PapersOnLine*, volume 56, 4484–4489. doi: 10.1016/j.ifacol.2023.10.938.

Schauer, T., Negård, N.O., Previdi, F., Hunt, K.J., Fraser, M.H., Ferchland, E., and Raisch, J. (2005). Online identification and nonlinear control of the electrically stimulated quadriceps muscle. *Control Engineering Practice*, 13(9), 1207–1219. doi: 10.1016/j.conengprac.2004.10.006.

Walsh, C. (2018). Human-in-the-loop development of soft wearable robots. *Nature Reviews Materials*, 3(6), 78–80. doi:10.1038/s41578-018-0011-1.

Weerdesteyn, V., de Niet, M., van Duijnhoven, H.J.R., and Geurts, A.C.H. (2008). Falls in individuals with stroke. *J. Rehabil. Res. Dev.*, 45(8), 1195–1214.

Winter, D.A. (2009). *Biomechanics and Motor Control of Human Movement: Fourth Edition*. New York: Wiley. doi:10.1002/9780470549148.